1	Long title: A revised understanding of Tribolium morphogenesis further
2	reconciles short and long germ development
3	
4	Short title: A significant revision to our understanding of short germ
5	embryogenesis
6	
7	
8	Author: Matthew A. Benton
9	
10	Author affiliation: Department of Zoology, University of Cologne, Cologne, NRW, Germany
11	
12	Corresponding author: Matthew A. Benton, matthewabenton@gmail.com

14 Author summary

15	In many animals, certain groups of cells in the embryo do not directly contribute to adult			
16	structures. Instead, these cells generate so-called 'extra-embryonic tissues' that support and			
17	facilitate development, but degenerate prior to birth/hatching. In most insect species,			
18	embryos are described as having two major extra-embryonic tissues; the serosa, which			
19	encapsulates the entire embryo and yolk, and the amnion, which covers one side of the			
20	embryo. This tissue structure has been widely reported for over a century, but detailed			
21	studies on the amnion are lacking. Working in the beetle Tribolium castaneum, I used long-			
22	term fluorescent live imaging, cell tracking and differential cell labelling to investigate			
23	amnion development. In contrast to our current understanding, I show that most cells			
24	previously thought to be amnion actually form large parts of the embryo. In addition, I show			
25	how these cells 'flow' as a whole tissue and contribute to elongation of the embryo, and how			
26	only a relatively small number of cells form the actual amnion. Lastly, I describe how my			
27	findings show that despite exhibiting substantial differences in overall structure, embryos of			
28	Tribolium and the fruit fly, Drosophila melanogaster, utilise a conserved set of			
29	morphogenetic processes.			

30

31 Abstract

In Drosophila melanogaster, the germband forms directly on the egg surface and solely consists of embryonic tissue. In contrast, most insect embryos undergo a complicated set of tissue rearrangements to generate a condensed, multi-layered germband. The ventral side of the germband is embryonic, while the dorsal side is thought to be an extraembryonic tissue called the amnion. While this tissue organisation has been accepted for decades, and has been widely reported in insects, its accuracy has not been directly tested in any species.

38	Using live cell tracking and differential cell labelling in the short germ beetle <i>Tribolium</i>			
39	castaneum, I show that most of the cells previously thought to be amnion actually give rise			
40	to large parts of the embryo. This process occurs via the dorsal-to-ventral flow of cells and			
41	contributes to germband extension. In addition, I show that true 'amnion' cells in Tribolium			
42	originate from a small region of the blastoderm. Together, my findings show that			
43	development in the short germ embryos of <i>Tribolium</i> and the long germ embryos of			
44	Drosophila is more similar than previously proposed. Dorsal-to-ventral cell flow also occurs			
45	in <i>Drosophila</i> during germband extension, and I argue that the flow is driven by a conserved			
46	set of underlying morphogenetic events in both species. Furthermore, the revised Tribolium			
47	fatemap that I present is far more similar to that of <i>Drosophila</i> than the classic <i>Tribolium</i>			
48	fatemap. Lastly, my findings show that there is no qualitative difference between the tissue			
49	structure of the cellularised blastoderm and the short/intermediate germ germband. As			
50	such, the same tissue patterning mechanisms could function continuously throughout the			
51	cellularised blastoderm and germband stages, and easily shift between them over			
52	evolutionary time.			

53

54 Introduction

Insects are the most speciose phylum of animals and display remarkable diversity in adult morphology [1]. Insect embryo development is also very diverse, particularly in the stages leading to the formation of the elongated, segmented embryo (called the germband) [2]. The molecular and morphogenetic basis of this process is best understood in the fly *Drosophila melanogaster*. In this species, a predominantly hierarchical chain of patterning events specifies nearly all segments more-or-less simultaneously at the syncytial blastoderm stage [3]. Cellularisation takes place near the end of this process, after which point

62 morphogenetic events such as germband extension (GBE) occur (see Fig 1 for schematic 63 summary). The *Drosophila* mode of development is termed long germ development and is 64 fairly representative of most true flies [4]. In contrast, the vast majority of insects undergo 65 short or intermediate germ development, meaning that only a handful of segments are 66 specified at the blastoderm stage and the remaining segments are specified sequentially as 67 the germband elongates [5].

68 Short germ development has been best studied in the beetle *Tribolium castaneum*, 69 and recent research has shown that development in this species is more similar to 70 Drosophila than previously thought. In Drosophila, GBE is predominantly driven by the 71 mediolateral intercalation of ectodermal cells (i.e. convergent extension), although cell 72 deformation along the anterior-posterior (AP) axis and cell divisions are also involved [6–11]. 73 In contrast to this, *Tribolium* germband elongation was previously thought to be driven by 74 the so-called 'growth zone' at the posterior of the germband [12]. Now, however, it is clear 75 that *Tribolium* germband elongation is also predominantly driven by mediolateral cell 76 intercalation (see Fig 1 for schematic summary of *Tribolium* development) [13–15]. 77 Furthermore, in both *Tribolium* and *Drosophila*, this intercalation requires the striped 78 expression of a specific group of Toll genes (so-called Long Toll/Loto class genes) [16,17]. 79 80 Fig 1. Schematics of development in Drosophila and Tribolium. The two left columns show 81 schematics of *Drosophila* embryos from the uniform blastoderm stage to the extended 82 germband stage. The right three columns show schematics of *Tribolium* embryos at

- 83 comparable developmental stages. The schematics in the right-most column depict
- 84 dissected, flatmounted embryos. Red arrows display cell/tissue movement. The question
- 85 marks highlight two regions (the *Drosophila* embryo/amnioserosa border in the cephalic

86	furrow region, and the dorsoventral position of the <i>Tribolium</i> embryo/amnion border) where		
87	the tissue boundaries are unknown/undescribed. Several features have been omitted,		
88	including the yolk, mesoderm gastrulation, anterior gut formation and appendage		
89	formation. The <i>Drosophila</i> fatemap is based on data from [18] and the references therein.		
90	Refer to text for additional details.		
91			
92	It is highly likely that germband elongation mediated by cell intercalation is		
93	homologous in these two species, and probably in other arthropods, as well [17]. As such, I		
94	will hereafter refer to <i>Tribolium</i> 'germband elongation' as 'germband extension'/GBE,		
95	unifying the <i>Drosophila/Tribolium</i> terminology. In addition, as there is no evidence for a		
96	qualitatively different 'growth zone' in <i>Tribolium</i> (i.e. a specialised zone of volumetric		
97	growth), I will refer to the posterior unsegmented region as the 'segment addition zone'		
98	(SAZ) [19–21].		
99	Despite the similarities described above, there are substantial differences in the		
100	embryonic fatemaps of these two species (Fig 1). In <i>Drosophila</i> , almost the entire		
101	blastoderm is fated as embryonic tissue, and only a small dorsal region is fated as		
102	extraembryonic tissue (termed the amnioserosa) [18]. In contrast, in <i>Tribolium</i> , roughly the		
103	anterior third of the blastoderm gives rise to an extraembryonic tissue called the serosa [22].		
104	Of the remaining blastoderm, a large dorsal region is thought to give rise to a second		
105	extraembryonic tissue called the amnion, with only the remaining ventral tissue giving rise to		
106	the embryo itself [23–25]. Like the amnioserosa, the serosa and the amnion are proposed to		
107	support the embryo during development, but are thought to degenerate prior to hatching		
108	and not contribute to any larval or adult structures [19,26,27].		

109	Drosophila and Tribolium also exhibit dramatic differences in the morphogenetic
110	events occurring during early development (Fig 1). When GBE occurs in Drosophila, the
111	germband stays at the surface of the egg and the amnioserosa largely remains in place. In
112	<i>Tribolium</i> , on the other hand, germband extension begins with a process called embryo
113	condensation, during which the embryonic ectoderm and presumptive amnion (together
114	termed the 'germ rudiment') form the germband (see Fig 1; for a detailed description see
115	[14,28]). Several concurrent morphogenetic events underlie embryo condensation. The
116	embryonic ectoderm condenses towards the ventral side of the egg via both mediolateral
117	cell intercalation and a cuboidal-to-columnar cell shape transition. Simultaneously, epithelial
118	folding and tissue involution occurs, causing the presumptive amnion to fold over the
119	embryonic ectoderm. During these movements, the serosa cells undergo a cuboidal-to-
120	squamous transition to spread over the entire egg surface. The final stage of embryo
121	condensation coincides with closure of the serosa (serosa window stage), which appears to
122	involve a supracellular actomyosin cable [14].
123	The differences in fatemap and tissue folding described above show that both
124	fatemap shifts and reductions in early morphogenetic events have contributed to the
125	evolution of the long germ mode of development found in <i>Drosophila</i> . However, it is
126	important to note that Drosophila, regarding the extraembryonic tissues, represents an
127	extreme case of reductive evolution, which is characteristic only for higher cylorrhaphan flies
128	[29]. More basally branching flies form both an amnion and a serosa, while still exhibiting
129	the long germ mode of development (for a review see [26]). For example, in the scuttle fly
130	Megaselia abdita, both an amnion and serosa form, but while the serosa spreads over the
131	egg surface as in <i>Tribolium</i> , the amnion remains at the dorsal side of the embryo, similar to
132	the <i>Drosophila</i> amnioserosa [30–33]. Such intermediate topologies help to explain the

evolution of the situation in *Drosophila*, where all extraembryonic cells remain at the dorsalside.

135 Understanding how these differences evolved is integral to understanding the shortto-long germ transition, but in order to study how this occurred, we first need to understand 136 137 how these tissues develop in each species. The form and function of the *Tribolium* serosa has 138 been analysed in several studies [22,34,35]. The amnion, on the other hand, has proven 139 harder to analyse, and the precise embryo/amnion boundary at the blastoderm stage is 140 unknown. However, a defined boundary between embryo and amnion has been proposed to 141 exist from when the germband forms (Fig 1) [23]. Cells in the ventral half of the germband 142 (ventral with respect to the germband dorsoventral [DV] polarity, but dorsal with respect to 143 the egg) are thought to give rise to all embryonic structures, while cells in the dorsal half of 144 the germband (dorsal with respect to the germband DV polarity, but ventral with respect to 145 the egg) are thought to form the amnion [25,36,37]. This germband structure has been 146 described in many insects over the past century and is proposed to represent the core 147 conserved structure of short/intermediate germ embryos (reviewed in [2,38,39]). However, 148 the proposed boundary between cells fated to become embryo and those fated to become 149 amnion has not been directly tested.

Here, I investigate the development of the presumptive amnion in *Tribolium* using a combination of fluorescent live imaging and fate mapping techniques. To my great surprise, I find that the majority of the cells previously described as 'amnion' actually form large parts of the embryo proper. Using fate-mapping experiments, I show that true 'amnion' cells originate from a very small domain of the blastoderm, just as the *Drosophila* amnioserosa cells do. I also show that the movement of cells from the 'amnion' side of the germband to the 'embryo' side of the germband occurs via the large scale flow of the ectodermal 157 epithelium. Lastly, I describe the underlying causes of this flow, and show how this tissue

158 movement is likely homologous to the dorsal-to-ventral tissue flow that occurs during

- 159 Drosophila GBE.
- 160
- 161 **Results**

162 Live cell tracking reveals movement of 'amnion' cells into the embryo

163 To examine the development of the *Tribolium* presumptive amnion in detail, I carried out

164 high resolution live imaging of embryos transiently labelled [14] with a fluorescent histone

165 marker (H2B-venus) to label nuclei. My goal was to track presumptive amnion cells from the

166 blastoderm stage onwards. However, it was not possible to accurately track the majority of

167 cells throughout embryo condensation and GBE, due to the extensive morphogenetic

rearrangements that take place during this process. Instead, I focused on the stage

immediately following condensation when the germband has formed, and analysed the

170 embryonic region where the presumptive amnion is closest to the surface of the egg.

171 Specifically, I tracked over 200 presumptive amnion cells from the central region of the

172 germband from the closure of the serosa window until after the formation of the thoracic

segments (over 11 hours of development; Fig 2 and S2 Movie). As previously described [14],

the germband and yolk exhibit pulsatile movements during this period, as well as rotatingwithin the serosa (S1 Movie).

The presumptive amnion initially consists of many tightly packed cells, which become increasingly spread out during GBE (S2 Movie, Fig 2(A-C)). However, rather than remaining restricted to the 'amnion territory', many of the tracked cells moved around the edge of the germband into the 'embryo territory'. Differential labelling of tracked cells clearly showed that these cells that moved around the germband edge became part of the embryo proper

(S2 Movie and Fig 2(A-C)). The cells that joined the 'embryo territory' became tightly packed,			
continued to divide, and formed embryonic structures (S3 Movie and Fig 2(D-F)). In contrast,			
cells that remained in the 'amnion territory' became squamous and stopped dividing. The			
nuclei of these latter cells became enlarged (S3 Movie and Fig 2(D-F)), suggesting that they			
underwent endoreplication to become polyploid, as seen in the <i>Tribolium</i> serosa and in the			
Drosophila amnioserosa [18,24]. In addition, several germband nuclei underwent apoptosis			
(S3 Movie) as has been described in fixed embryos [40]. These results show that many of the			
cells previously thought to constitute extraembryonic amnion give rise to embryonic			
structures.			
Since the epithelium formerly termed 'amnion' is made up cells that will variously			
form amnion, dorsal ectoderm and dorsolateral ectoderm, it is not accurate for the entire			
tissue to be called 'amnion'. Therefore, I will refer to this part of the germband as the 'dorsal			
epithelium', based on the tissue's location at the dorsal side of the germband (with respect			
to the DV polarity of the germband rather than the egg). This term 'dorsal epithelium' is			
simply a spatial designation, and comes with no implicit assumptions about the identity of			
the tissue nor the final fate of the tissue. It is also important to keep in mind that the dorsal			
epithelium is continuous with the ventral epithelium.			
Fig 2. Live cell tracking reveals contribution of 'amnion' cells to embryonic tissue. (A-F)			
Time series from fluorescent live imaging of a <i>Tribolium</i> embryo expressing H2B-venus. The			
serosa nuclei located above the germband have been manually removed from these frames			

- 202 (by deleting them from individual z-stack slices), but left in the surrounding territory
- 203 (arrowhead in (A+A')). (A'-C') show optical transverse sections of the respective frame at the
- 204 position shown by the dashed line (the surface of the egg is to the left). In (A-C), all nuclei

205 that lie in a region of the 'amnion territory' in (A) have been tracked and differentially 206 labelled depending on whether they become part of the embryo (magenta; labels disappear 207 when nuclei join the germband), become located at the edge of the germband (yellow) or 208 remain in the 'amnion territory' (cyan). In (D-F), a line of nuclei that lie in the 'amnion 209 territory' in (D) have been tracked and differentially labelled depending on whether they 210 become part of the embryo (coloured points; daughter cells are labelled in same colour as 211 parent) or remain in the 'amnion territory' (cyan; no division takes place). Note that in panel 212 (D), the orange spot is mostly hidden below the yellow spot because the nuclei in that region 213 are partially overlapping when viewed as projections. The first frame of the timelapse was 214 defined as timepoint 0. In (A-F), embryos are oriented based on the AP/DV polarity of the 215 egg with anterior to the left and dorsal to the top. (A-C) are maximum intensity projections 216 of one egg hemisphere. (D-F) are average intensity projections of 46 microns to specifically 217 show the germband. Scale bars are $50 \, \mu m$.

218

219 Differential cell labelling confirms widespread dorsal-to-ventral cell movement

220 My next question was whether the movement of cells from the dorsal epithelium to the 221 ventral epithelium occurs throughout the AP axis or is just limited to the thoracic region. The 222 extensive movements of the germband made it difficult to track individual cells accurately at 223 the anterior and posterior poles. To overcome this problem, I combined differential cell 224 labelling with long term fluorescent live imaging to follow small groups of nuclei throughout 225 development. Specifically, I microinjected mRNA encoding a nuclear-localised 226 photoconvertable fluorescent protein (NLS-tdEos) into pre-blastoderm embryos to uniformly 227 label all nuclei, then photoconverted a small patch of nuclei at different positions along the 228 AP axis at the final uniform blastoderm stage. I then performed long term confocal live

229 imaging of both the unconverted and photoconverted forms of the fluorescent protein 230 throughout the period of GBE (or longer). Unlike that of Drosophila, the Tribolium egg shell 231 does not show any dorsoventral (DV) polarity, and I was therefore unable to specifically 232 target particular locations along the DV axis. Instead, I opted for a brute-force approach and 233 performed the photoconversion experiment at unknown DV positions for 50-150 embryos at 234 each of the following AP positions: 75% egg length (EL) from the posterior pole, 50% EL, 25% 235 EL, and close to the posterior pole. I then used the resulting live imaging data to determine 236 the approximate DV position of the photoconverted cells. Using a new live imaging set up 237 (see Materials and Methods), I obtained the same range of hatching rates as I typically 238 obtain for other microinjection experiments (approximately 80%, [14]), even after 239 continuous confocal live imaging for almost the entirety of *Tribolium* embryonic 240 development (3.5 days; S4 Movie). Both unconverted and photoconverted protein persisted 241 throughout germband extension and retraction, although fluorescent signal faded over time. 242 I have included various examples from this data set in S1-S3 Figures. In addition, I have made 243 the raw confocal data for a large number of timelapses available online (>300 embryos, >700 244 GB of data [41]) for the benefit of the community. This data will likely prove valuable for a 245 wide range of research projects. 246 When I examined clones initially located in the dorsal epithelium, I found that 247 movement of cells from the dorsal epithelium to the ventral epithelium occurred throughout

the posterior of the embryo during GBE (Fig 3(A-F), S5 Movie). I also observed the same

249 movements at the anterior of the germband (Fig 3(G-J)), although I have focused my analysis

- on the middle and posterior parts of the embryo. Together with the cell tracking data, these
- 251 results show that most of what was previously thought to be 'amnion' is in fact embryonic

tissue, and that cells move from the dorsal epithelium to the ventral epithelium throughoutthe germband (summarised in Fig 3(K,L)).

254

255 Fig 3. Differential cell labelling reveals widespread movement of cells from the dorsal 256 epithelium to the ventral epithelium. (A-J) Time series from fluorescent live imaging of two 257 Tribolium embryos expressing NLS-tdEos showing unconverted protein (magenta) and 258 photoconverted protein (cyan). In (A-F') a patch of nuclei at the posterior-dorsal region of 259 the blastoderm were photoconverted. Panels (A-F) show the posterior region of the 260 germband during late GBE and panels (A'-F') show optical transverse sections made at the 261 position of the dashed line at each timepoint (roughly following the same nuclei). Serosa 262 nuclei are marked by white crosses in the transverse sections. In (G-J), a patch of nuclei at 263 the anterior-lateral region of the blastoderm were photoconverted. Panels (G-J) show the 264 anterior of the germband during condensation and GBE. In both embryos, all converted 265 nuclei are initially located in the dorsal epithelium, but most move into the ventral 266 epithelium during GBE. (K-L) Schematics showing the classic and revised models of the 267 Tribolium germband (presumptive amnion is shown in purple, presumptive embryo is shown 268 in grey, red arrows show the newly discovered tissue flow). The first frame of the timelapses 269 was defined as timepoint 0. In (A-J), embryos are oriented based on the AP/DV polarity of 270 the egg with anterior to the left and dorsal to the top. In (A'-F'), the surface of the egg is 271 oriented to the left. In (K-L), schematics show flatmounted germbands with the focus on the 272 dorsal epithelium, the anterior to the left and the orthogonal sections are oriented with the 273 dorsal half of the germband to the left. (A-J) are maximum intensity projections of one egg 274 hemisphere. Scale bars are 50 µm.

275

276 Mediolateral cell intercalation occurs throughout GBE

277	During my live imaging, ectodermal cell clones became elongated along the AP axis over		
278	time, as previously reported in a <i>Tribolium</i> study that used a non-live imaging cell clone		
279	method [15]. However, this study found that "labelled ectodermal cells rarely mix with		
280	unlabelled cells" even as clones became greatly elongated [15]. In contrast, I frequently		
281	observed non-converted nuclei in the midst of labelled nuclei (Fig 3, S1-S3 Figs).		
282	To test whether the pattern I observed was caused by mediolateral cell intercalation,		
283	I tracked the nuclei of abutting rows of ectodermal cells in the SAZ during formation of the		
284	abdominal segments (50 cells in total, tracked for 3.5 hours; Fig 4 and S6 Movie). This		
285	analysis clearly showed that, as during embryo condensation [14], cells intercalated between		
286	their dorsal and ventral neighbours. Together with the photoconversion dataset, these		
287	results show that extensive mediolateral cell intercalation takes place throughout GBE to		
288	drive the convergent extension of the ectoderm.		
289			
290	Fig 4. Mediolateral cell intercalation occurs in the SAZ during GBE. Time series from		
291	fluorescent live imaging of a <i>Tribolium</i> embryo expressing NLS-tdEos showing the SAZ during		
292	abdominal segment formation. Coloured points mark tracked nuclei. During the timelapse,		
293	nuclei underwent apicobasal movement but I observed no cell delamination. Note that the		
294	same embryo is shown in Fig 3(A-F). The first frame of the timelapse was defined as		
295	timepoint 0. The embryo is oriented based on polarity of the visible region of the germband.		

296 Panels show maximum intensity projections of 15 μm to specifically show the germband.

297 Abbreviations as follows: germband (GB); anterior (ant); posterior (post); medial (med);

298 lateral (lat). The scale bar is 50 μm.

299

300 Tribolium serpent may mark true 'amnion'

301	As described earlier, cells that remained in the dorsal epithelium became squamous, and this			
302	cell shape change occurred progressively along the AP axis (Fig 5(A)). This change in cell			
303	shape may be a sign of maturation of true 'amnion'. While characterising cell fate markers, I			
304	found that the <i>Tribolium</i> ortholog of the GATA factor <i>serpent</i> (<i>Tc-srp</i>) exhibited spatial and			
305	temporal expression dynamics that were very similar to those of the potential 'amnion' (i.e.			
306	progressive flattening of cells, Fig 5(B), S4 Fig).			
307	At the end of GBE, all but the most posterior cells of the dorsal epithelium were			
308	squamous and <i>Tc-srp</i> seemed to be expressed in dorsal epithelium cells along nearly the fo			
309	length of the germband (S4 Fig(I_2)). However, this latter finding was difficult to confirm as			
310	most of the dorsal epithelium is lost during embryo fixation at this embryonic stage			
311	(presumably due to the fragility of the tissue). I also found <i>Tc-srp</i> to be expressed in several			
312	other domains, including in the presumptive endoderm (S4 Fig).			
313	In <i>Drosophila, serpent</i> is also expressed in extraembryonic tissue (the amnioserosa)			
314	[42–45], and, therefore, <i>Tc-srp</i> may mark 'true' extraembryonic amnion. However, future			
315	work is required to confirm whether this putative amnion degenerates prior to hatching (as			
316	is required to be defined as extraembryonic). For simplicity, I will refer to this tissue as			
317	'amnion' for the remainder of this text.			
318				
319	Fig 5. Development of the putative amnion. (A-A") Tribolium embryo transiently expressing			
320	the membrane marker GAP43-YFP. (A) shows an overview of the whole egg, (A') shows the			
321	dorsal epithelium of the same embryo at the position of the white box, (A $^{\prime\prime}$) is an optical			
322	sagittal section at the position of the dashed line in (A') showing the apical-basal height of			
323	cells of the dorsal epithelium. (B) <i>Tc-srp</i> (red) expression in a flatmounted <i>Tribolium</i>			

324 germband also showing nuclei (DAPI, blue). The strong *Tc-srp* signal in nuclei may suggest 325 nuclear or peri-nuclear localisation of the transcript, or it may be due to the cell body being 326 flattened. Aside from the strong patch of anterior medial expression (which is from cells 327 beneath the embryonic ectoderm), all visible expression is in the putative amnion 328 epithelium. (C-E) Extended germband stage Tribolium embryos transiently expressing NLS-329 tdEos showing unconverted protein (magenta) and photoconverted protein (cyan). In each 330 embryo, the clone of converted cells spans the entire amnion. $(C_{1,2})$ show both sides of the 331 same embryo in which a 6 nuclei wide patch of dorsal-most cells located at 50% EL were 332 photoconverted at the blastoderm stage. (D) shows an embryo in which a 3 nuclei wide 333 patch of dorsal-most cells located at 25% EL were photoconverted at the blastoderm stage. 334 (E) shows an embryo in which a 3 nuclei wide by 6 nuclei long patch of dorsal-most cells 335 located at roughly 2-10% EL were photoconverted at the blastoderm stage. In (A) and (C-E), 336 embryos are oriented based on the AP/DV polarity of the egg with anterior to the left and 337 dorsal to the top. In (A''), the surface of the egg is oriented to the bottom. In (B), the anterior 338 of the germband is to the left. (A) is an average intensity projection of one egg hemisphere. 339 (A') is an average intensity projection of 6 μ m to specifically show the dorsal epithelium. (B) 340 is a maximum intensity projection of the whole germband. (C-E) are maximum intensity 341 projections of one egg hemisphere. Abbreviations are: ventral ectoderm (VE) and dorsal 342 ectoderm (DE). Scale bars are $50 \,\mu m$.

343

344 A revised *Tribolium* amnion fatemap

To determine which blastoderm cells give rise to the amnion, I analysed 85 embryos in which

the dorsal and dorsolateral blastoderm cells were labelled by NLStdEos photoconversion as

347 described above. As I was unable to determine the precise DV position of the

348 photoconverted cells at the blastoderm stage, I (1) examined embryos at the extended 349 germband stage (when the mature amnion had formed), (2) determined the embryos in 350 which photoconverted nuclei spanned the full DV width of the amnion (but were not 351 observed in the embryonic tissue), and (3) checked the initial size of the photoconverted 352 patch of nuclei (for a schematic of this approach, see <mark>S</mark>5 Fig). 353 I found that amnion cells arose from a very small domain of dorsal-most cells (that 354 tapers from its anterior to posterior extent) and from a narrow strip of cells between the 355 presumptive embryo and presumptive serosa (summarised in Fig 6 and S6 Fig). At 50% EL, 356 only approximately the 6 most dorsal cells (approximately 8% of the circumference of the 357 blastoderm) gave rise to all amnion cells stretching from one side of the thorax to the other 358 (Fig 5(C), S1 Fig). Nearer to the posterior of the blastoderm (25% EL), even fewer cells gave 359 rise to amnion (approximately 3 of the most dorsal cells; approximately 6% of the 360 circumference; Fig 5(D), S2 Fig). The posterior limit of the amnion was difficult to define, as 361 although some cells from approximately 5-10% EL appeared to become amnion (Fig5(E)), 362 these cells condensed posteriorly towards the hindgut during germband retraction, and 363 might have contributed to the hindgut tissue (S3 Fig, S7 Movie). I was unable to 364 unambiguously determine the fate of these cells. At the anterior of the embryo, I found that 365 a narrow strip of 1-2 cells between the presumptive embryo and presumptive serosa also 366 gave rise to amnion (Fig 3(G-J)). While substantial additional work will be required to define 367 a complete blastoderm fatemap for Tribolium, my findings clearly demonstrate that the 368 'amnion' domain is drastically smaller than previously proposed. 369

Fig 6. Schematics showing the revised *Tribolium* amnion fatemap and germband model.
Schematics drawn as in Fig 1 to show the revised fatemap (top row; drawn directly from the

372	numbers described in the text) and germband model based on the results of this manuscript.		
373	Note that the posterior amnion/embryo boundary is unclear. The schematics of the		
374	flatmounted germbands are drawn with the focus on the dorsal epithelium. See text for		
375	additional details, and S6 Fig for an extended figure with the classic and revised models side-		
376	by-side.		
377			
378	Discussion		
379	In this article, I have shown that a majority of the cells currently thought to be		
380	extraembryonic amnion actually give rise to embryonic tissue. Movement of these cells from		
381	the dorsal side of the germband to the ventral side was visible in live cell tracking and		
382	differential cell labelling experiments. My results also indicate that the true amnion region		
383	differentiates progressively along the AP axis during GBE, as evidenced by differences in cell		
384	behaviour and the expression of the gene <i>Tc-srp</i> . Lastly, presumptive amnion cells		
385	predominantly originate from a small domain on the dorsal side of the blastoderm.		
386			
387	A revised understanding of the short germ embryo		
388	The revision to the <i>Tribolium</i> blastoderm fatemap that I describe is essentially a quantitative		
389	shift in our understanding of where cell fate boundaries lie along the DV axis. In the revised		
390	fatemap (Fig 6, S6 Fig), the proportion of the blastoderm that gives rise to the presumptive		
391	amnion is much smaller than previously thought. The presumptive amnion domain is,		
392	therefore, remarkably similar in size to the amnioserosa domain of the Drosophila		
393	blastoderm fatemap [18]. However, it is important to recognize that fatemaps such as those		
394	presented here show a static picture of a dynamic process. There is no evidence that the		
395	presumptive amnion is specified at the blastoderm stage in Tribolium. Instead, the		

396 progressive changes in cell shape and activation of *Tc-srp* expression in the dorsal epithelium 397 of the germband suggest that the amnion is specified progressively along the AP axis during 398 GBE. Progressive specification of DV cell fates during GBE fits with previous hypotheses 399 [36,46], and analysis of how this process occurs represents an exciting avenue of future 400 research (a possible mechanism for DV patterning during GBE is discussed in S1 Text). 401 In contrast to the fatemap revision, the observation that cells move from the dorsal 402 half of the germband to the ventral half of the germband represents a qualitative shift in our 403 understanding of development in short/intermediate germ insects. In the classic model of 404 short/intermediate germ development, the germband was thought of as a more-or-less flat 405 sheet of ectodermal cells (with mesoderm underneath) covered by the extraembryonic 406 amnion. Because of this, the entire dorsal epithelium is routinely removed during embryo 407 preparation, or not included in descriptions of gene expression patterns and embryonic 408 phenotypes. Based on the new data presented here, it is obvious that we have been 409 discarding or ignoring large parts of the embryo. Furthermore, the movement of cells from 410 the dorsal epithelium into the ventral epithelium must be contributing to GBE, and is, 411 therefore, a key aspect of the extension and overall development of the germband that has 412 thus far been missed. 413 The revised model of the germband does present some technical challenges for 414 future work on short/intermediate germ embryo. The flattened geometry of the germband 415 makes it difficult to image both the dorsal and ventral epithelium using bright-field 416 microscopy approaches. However, this problem can be overcome either by using 417 fluorescence based techniques and confocal microscopy or by mechanical sectioning of the germband. Both approaches have been shown to work well in Tribolium (for examples see 418

419 [13,47] and the results in this manuscript). In the rest of this article, I discuss why the revised

fatemap and cell flow accord well with what we know about *Tribolium* development, and
outline the implications of this discovery on our understanding of the evolution of insect
development.

423

424 The cellular and molecular causes of tissue flow unify the blastoderm and the germband 425 The revised model of the Tribolium germband reconciles the blastoderm and germband 426 stages. The ectoderm of the germband is a continuous epithelium, which means that the 427 movement of cells from the dorsal epithelium to the ventral epithelium occurs as a tissue 428 level 'flow'. Such dorsal-to-ventral tissue flow also occurs during embryo condensation in 429 Tribolium [14], and I propose that the flow is caused by largely the same morphogenetic 430 processes at both stages. The evidence for this hypothesis is summarised here, but for an 431 extended discussion see S2 Text. 432 Three morphogenetic processes contribute to dorsal-to-ventral cell flow in *Tribolium*,

433 and at least two of the three occur at both the blastoderm and germband stages. First, 434 mediolateral cell intercalation occurs at both stages and causes tissue-wide convergence 435 (along the DV axis) and extension (along the AP axis). This process requires two Toll genes 436 that are expressed in rings around the entire blastoderm and germband epithelium [17]. 437 Second, tissue specific cell shape changes occur at both stages such that ventral/lateral cells 438 become columnar and dorsal/dorsolateral cells become thinner (during condensation (S7 Fig 439)) or squamous (during GBE). The tissue level effect of these changes is contraction of the 440 ventral/lateral ectoderm and spreading of the dorsal tissue. The flattening of 441 dorsal/dorsolateral cells is likely regulated by BMP signalling, as not only does BMP activity correlate with the cell shape changes (see S2 Text), but functional disruption of BMP 442 443 signalling components leads to uniform cell shape changes along the DV axis [25,48]. A third

major morphogenetic event is gastrulation of the mesoderm. This occurs along the ventral
midline, and as gastrulation occurs, the ectoderm moves ventrally to seal the gap left in the
epithelium [47]. At the stage when a complete germband has formed, gastrulation is
complete along most of the embryo. However, current data suggests mesoderm gastrulation
may be ongoing in the SAZ [47]. If true, the ongoing invagination would contribute to tissue
flow in this region.

450 It is important to note that while each of the events described here is involved in the 451 dorsal-to-ventral tissue flow, no single event is absolutely required for it. In the absence of 452 cell intercalation, embryo condensation and thinning of dorsal/dorsolateral ectoderm still 453 takes place, yielding abnormally wide and short germbands [17]. In the absence of tissue 454 specific cell shape changes, condensation occurs in a more radially symmetrical manner 455 yielding a tube-shaped germband that undergoes segment specification and convergent 456 extension [25,48]. Finally, both condensation and GBE are only mildly affected in the 457 absence of mesoderm specification [49]. This functional independence comes from each of 458 the three processes being specified by different pathways (intercalation via segment 459 specification, dorsal thinning via dorsal tissue specification, and gastrulation via ventral 460 tissue specification). There may also be further, as yet undiscovered, morphogenetic events 461 which also contribute to the dorsal-to-ventral tissue flow. 462

463 **Reconciling long and short germ development**

464 I propose that the dorsal-to-ventral tissue flow occurring during embryo condensation and

465 GBE in *Tribolium* is homologous to the dorsal-to-ventral tissue flow that occurs during

466 gastrulation and GBE in *Drosophila* (Fig 1). This conclusion is based on the flow being driven

467 by a conserved set of morphogenetic events.

468 As described above, tissue flow in *Tribolium* is caused by (1) mediolateral cell 469 intercalation, (2) tissue specific cell shape changes along the DV axis, and (3) gastrulation at 470 the ventral side of the embryo. As described below, equivalent processes are all observed in 471 Drosophila as well. 472 In Drosophila, Toll-mediated mediolateral cell intercalation causes tissue-wide convergence (along the DV axis) and extension (along the AP axis) of the ectoderm during 473 474 GBE [16]. As in *Tribolium*, the periodic expression of the *Toll* genes is regulated by the pair-475 rule genes. Conservation at the level of tissue identity, morphogenetic process, and 476 molecular control strongly suggest *Toll*-mediated cell intercalation to be homologous. 477 Cell shape changes are harder to compare between Drosophila and Tribolium, 478 because unlike in most insects, cellularisation in *Drosophila* leads to the direct formation of 479 columnar cells [18,50]. However, tissue-specific cell shape changes along the DV axis do 480 occur in *Drosophila* and are dependent on BMP signalling ([51,52]; for a detailed description 481 see S3 Text). While the intracellular effectors of these cell shape changes are unknown, use 482 of BMP signalling for dorsal patterning is homologous in *Drosophila* and *Tribolium*, and many 483 dorsal cell specification genes are conserved between these two species [48]. 484 Last, Drosophila mesoderm gastrulation also occurs along the ventral midline, and 485 causes lateral/dorsolateral ectoderm to move ventrally [51]. Similar to the tissue specific cell 486 shape changes described above, the intracellular effectors of *Tribolium* mesoderm 487 gastrulation are unknown, but the upstream patterning events and the tissue specification 488 genes are highly conserved [36,49]. Furthermore, mesoderm gastrulation at the ventral 489 region of the embryo is widely observed within the insects, and is undoubtedly a 490 homologous process in each species [53].

491	While I have focused on <i>Tribolium</i> and <i>Drosophila</i> here, evidence exists that
492	the new findings in <i>Tribolium</i> may also apply to other short/intermediate germ insects. For
493	example, in the intermediate germ bug Oncopeltus fasciatus (which forms a condensed,
494	multi-layered germband with tissue topology similar to that of <i>Tribolium</i> [26]), the dorsal
495	epithelium of the germband initially consists of a thick epithelium which progressively
496	becomes squamous late during GBE [54]. These tissue-specific cell shape changes are likely
497	the same as those occurring during <i>Tribolium</i> GBE. Furthermore, <i>Oncopeltus</i> pair-rule genes,
498	Loto Toll genes and even segment polarity genes are expressed in rings around the entire
499	germband prior to thinning of the dorsal epithelium [17,55,56]. The expression of these
500	genes in the dorsal epithelium provides additional evidence that much of the Oncopeltus
501	dorsal epithelium is made up of embryonic tissue. Future analyses of the molecular and
502	morphogenetic drivers of GBE must analyse the entire germband, rather than focusing on
503	the ventral half. In addition, further work will be needed to determine whether the new
504	findings in <i>Tribolium</i> also apply to more basally branching insects such as crickets.
505	

506 Materials and Methods

507 *Tribolium* animal husbandry, egg collection, and RNA *in situ* hybridisation was performed as

previously described [17]. The *Tc-srp* ortholog was previously described [57] and was cloned

509 into pGEM-t (Promega Reference A1360) with primers TCCCGCTGCTTTGATCTAGT and

510 TGCGATGACTGTGACGTGTA. The *Tc-cad* ortholog was as previously used [14].

511 The *H2B-ven* fusion was created by fusing the *D. melanogaster* histone *H2B* coding

sequence (without the stop codon) from the published H2B-RFP [14] to the *venus*

513 fluorescent protein [58] and cloning into the pSP64 Poly(A) (Promega Reference P1241)

514 expression vector. The *NLS-tdEos* fusion was kindly provided by Matthias Pechmann.

515 Additional details and both plasmids are available upon request to M. Pechmann or myself. 516 Capped mRNA synthesis was performed as previously described [14]. H2B-ven capped mRNA 517 was injected at 1 μ g/ μ L, *NLS-tdEos* capped mRNA was injected at 2-3 μ g/ μ L. 518 Embryo microinjection was performed as previously described [14], with the 519 following changes. Up to 100 dechorionated embryos were mounted on a rectangular 520 coverslip (24 mm by 50 mm) that rested on a microscope slide. Water was allowed to dry off 521 the embryos before they were covered in Voltalef 10S halocarbon oil and injected as usual. 522 The coverslip (still resting on the slide) was then placed in a petri-dish (92 mm) containing a 523 base layer of 1% agarose (dissolved in water) and placed at 30-32°C until the embryos were 524 at the appropriate stage for imaging. The coverslip was then removed from the slide, 525 inverted (so that embryos were face down), and quickly but gently placed on a lumox dish 526 (50 mm; Sarstedt Reference 94.6077.410) that was sitting upside down. The corners of the 527 coverslip rested on the raised plastic lip of the dish such that the membrane and embryos 528 were close to each other but not touching. To ensure lateral stability of the coverslip during 529 the timelapse recording, approximately 5-10 μ L of heptane glue (made by soaking parcel 530 tape in heptane) was placed at each corner. Additional Voltalef 10S halocarbon oil was then 531 added to fill any remaining space between the coverslip and the oxygen permeable 532 membrane. This contraption was then stuck to a microscope slide (using double sided tape) 533 for imaging on an upright microscope. This last step may be unnecessary depending on the 534 microscope stage and orientation. 535 Live imaging was performed on an upright Zeiss SP8 confocal microscope equipped 536 with Hybrid detectors in the Biocentre Imaging facility (University of Cologne). Image stacks

537 $\,$ of 15-50 focal planes with z-steps ranging from 2-10 μm were taken with a 10x/0.3NA dry

538 objective or a 20×/0.7NA multi-immersion objective at intervals of 5-45 minutes. The

temperature of the sample during imaging could not be carefully regulated, but was typically
between 25-28 degrees. While this lack of temperature control is not ideal, it does not affect
the findings presented in this manuscript.

542 Photoconversion of NLS-tdEos protein was performed by constantly scanning the 543 region of interest for 20-30 seconds with the 405 wavelength laser at low power (5%). These 544 settings were manually determined on the above microscope, and need to be determined 545 independently on different systems. Photoconversions were performed during the final 546 uniform blastoderm stage, as photoconversion prior to this resulted in substantial diffusion 547 of the photoconverted protein during nuclei division. The positions of the different regions 548 of the embryo (75% EL etc.) were determined by measuring the length of each embryo in the 549 LASX software and selecting the appropriate region. Photoconversions were performed on 550 all embryos on the coverslip before setting up the timelapse, which led to a 0.5-2 hour delay 551 between performing the photoconversion and beginning the timelapse. As such, the 552 positions of the photoconverted region at the first time point in the timelapses in this 553 manuscript do not reflect the original region of photoconversion. 554 Imaging of fixed material was performed on an upright Zeiss SP8 confocal, an upright 555 Zeiss SP5 confocal microscope and an inverted Zeiss SP5 confocal microscope. The 556 Drosophila gooseberry expression patterns were kindly provided by Erik Clark and acquired 557 as in [59]. Images and timelapses were analysed using FIJI [60] and Photoshop CS5. Manual 558 cell tracking was performed on confocal hyperstacks with MTrackJ [61]. The figures were 559 arranged and the schematics created using Inkscape. 560

561 Acknowledgements

562	l am v	ery grateful to S. Roth for his generous support, and for the extensive and stimulating	
563	discussions throughout this project. I am also thankful to E. Clark for in-depth discussions		
564	and extensive feedback on the manuscript. I thank M. Pechmann for providing the NLS-tdEos		
565	construct. In addition, I thank M. Akam, M. Pechmann and S. Roth for comments on the		
566	manuscript, and B. Schmitt for comments on the schematics.		
567			
568	References		
569	1.	Grimaldi D, Engel M. Evolution of the Insects. Cambridge University Press; 2005.	
570	2.	Anderson DT. Embryology and Phylogeny in Annelids and Arthropod. Pergamon Press;	
571		1973.	
572	3.	Jaeger J. The gap gene network. Cell Mol Life Sci. 2011;68: 243–74.	
573		doi:10.1007/s00018-010-0536-y	
574	4.	Davis GK, Patel NH. SHORT, LONG, AND BEYOND: Molecular and Embryological	
575		Approaches to. Annu Rev Entomol. 2002; 669–99.	
576	5.	Peel AD, Chipman AD, Akam M. Arthropod segmentation: beyond the Drosophila	
577		paradigm. Nat Rev Genet. 2005;6: 905–16. doi:10.1038/nrg1724	
578	6.	Irvine KD, Wieschaus E. Cell intercalation during Drosophila germband extension and	
579		its regulation by pair-rule segmentation genes. Development. 1994;120: 827–41.	
580		Available: http://www.ncbi.nlm.nih.gov/pubmed/7600960	
581	7.	Bertet C, Sulak L, Lecuit T. Myosin-dependent junction remodelling controls planar cell	
582		intercalation and axis elongation. Nature. 2004;429: 667–671. Available:	
583		http://dx.doi.org/10.1038/nature02590	
584	8.	Collinet C, Rauzi M, Lenne P, Lecuit T. Local and tissue-scale forces drive oriented	
585		junction growth during tissue extension. Nat Cell Biol. 2015;17: 1247–1258.	

586	doi:10.1038/ncb3226
-----	---------------------

587	9.	Butler LC, Blanchard GB, Kabla AJ, Lawrence NJ, Welchman DP, Mahadevan L, et al.
588		Cell shape changes indicate a role for extrinsic tensile forces in Drosophila germ-band
589		extension. Nat Cell Biol. Nature Publishing Group; 2009;11: 859–64.
590		doi:10.1038/ncb1894
591	10.	Firmino AAP, Fonseca FC de A, de Macedo LLP, Coelho RR, Antonino de Souza Jr JD,
592		Togawa RC, et al. Transcriptome Analysis in Cotton Boll Weevil (Anthonomus grandis)
593		and RNA Interference in Insect Pests. PLoS One. 2013;8: e85079.
594		doi:10.1371/journal.pone.0085079
595	11.	da Silva SM, Vincent J-P. Oriented cell divisions in the extending germband of
596		Drosophila Development. 2007;134: 3049 LP-3054. Available:
597		http://dev.biologists.org/content/134/17/3049.abstract
598	12.	Liu PZ, Kaufman TC. Short and long germ segmentation: unanswered questions in the
599		evolution of a developmental mode. Evol Dev. 2005;7: 629–46. doi:10.1111/j.1525-
600		142X.2005.05066.x
601	13.	Sarrazin AF, Peel AD, Averof M. A segmentation clock with two-segment periodicity in
602		insects. Science. 2012;336: 338–41. doi:10.1126/science.1218256
603	14.	Benton MA, Akam M, Pavlopoulos A. Cell and tissue dynamics during Tribolium
604		embryogenesis revealed by versatile fluorescence labeling approaches. Development.
605		2013;140: 3210–3220. doi:10.1242/dev.096271
606	15.	Nakamoto A, Hester SD, Constantinou SJ, Blaine WG, Tewksbury AB, Matei MT, et al.
607		Changing cell behaviours during beetle embryogenesis correlates with slowing of
608		segmentation. Nat Commun. Nature Publishing Group; 2015;6: 6635.

609 doi:10.1038/ncomms7635

- 610 16. Paré AC, Vichas A, Fincher CT, Mirman Z, Farrell DL, Mainieri A, et al. A positional Toll
- 611 receptor code directs convergent extension in Drosophila. Nature. 2014;515: 523-
- 612 527. doi:10.1038/nature13953
- 613 17. Benton MA, Pechmann M, Frey N, Stappert D, Conrads KHKH, Chen Y-TY-T, et al. Toll
- 614 Genes Have an Ancestral Role in Axis Elongation. Curr Biol. Elsevier Ltd; 2016;26:
- 615 1609–1615. doi:10.1016/j.cub.2016.04.055
- 616 18. Campos-Ortega J a, Hartenstein V. The embryonic development of Drosophila
- 617 melanogaster. 2nd ed. Springer-Verlag Berlin Heidelberg; 1997.
- 19. Schönauer A, Paese CLB, Hilbrant M, Leite DJ, Schwager EE, Feitosa NM, et al. The Wnt
- and Delta-Notch signalling pathways interact to direct pair-rule gene expression via
- 620 caudal during segment addition in the spider Parasteatoda tepidariorum.
- 621 Development. 2016; 2455–2463. doi:10.1242/dev.131656
- 622 20. Janssen R. Gene expression suggests double-segmental and single-segmental
- 623 patterning mechanisms during posterior segment addition in the beetle Tribolium
- 624 castaneum. Int J Dev Biol. 2014;58. doi:10.1387/ijdb.140058rj
- 625 21. Clark E. Dynamic patterning by the Drosophila pair-rule network reconciles long-germ
- and short-germ segmentation. Desplan C, editor. PLOS Biol. 2017;15: e2002439.
- 627 doi:10.1371/journal.pbio.2002439
- 628 22. van der Zee M, Berns N, Roth S. Distinct Functions of the Tribolium zerknullt Genes in
- 629 Serosa Specification and Dorsal Closure. Curr Biol. 2005;15: 624–636.
- 630 doi:10.1016/j.cub.2005.02.057
- 631 23. Falciani F, Hausdorf B, Schröder R, Akam M, Tautz D, Denell R, et al. Class 3 Hox genes

in insects and the origin of zen. Proc Natl Acad Sci USA. 1996;93: 8479–8484.

633 24. Handel K, Grünfelder CG, Roth S, Sander K. Tribolium embryogenesis: a SEM study of

- 634 cell shapes and movements from blastoderm to serosal closure. Dev Genes. 2000;
- 635 25. Nunes da Fonseca R, von Levetzow C, Kalscheuer P, Basal A, van der Zee M, Roth S.
- 636 Self-Regulatory Circuits in Dorsoventral Axis Formation of the Short-Germ Beetle
- 637 Tribolium castaneum. Dev Cell. 2008;14: 605–615.
- 638 doi:https://doi.org/10.1016/j.devcel.2008.02.011
- 639 26. Schmidt-Ott U, Kwan CW. Morphogenetic functions of extraembryonic membranes in
- 640 insects. Curr Opin Insect Sci. Elsevier Inc; 2016;13: 86–92.
- 641 doi:10.1016/j.cois.2016.01.009
- 642 27. Panfilio K a. Extraembryonic development in insects and the acrobatics of
- 643 blastokinesis. Dev Biol. 2008;313: 471–91. doi:10.1016/j.ydbio.2007.11.004
- 644 28. Benton MA, Pavlopoulos A. Tribolium embryo morphogenesis: May the force be with

645 you. Bioarchitecture. 2014;4: 16–21. doi:10.4161/bioa.27815

646 29. Schmidt-Ott U. The amnioserosa is an apomorphic character of cyclorrhaphan flies.

647 Dev Genes Evol. 2000;210: 373–376. doi:10.1007/s004270000068

- 648 30. Rafiqi AM, Lemke S, Ferguson S, Stauber M, Schmidt-Ott U. Evolutionary origin of the
- 649 amnioserosa in cyclorrhaphan flies correlates with spatial and temporal expression
- 650 changes of zen. Proc Natl Acad Sci U S A. 2008;105: 234–9.
- 651 doi:10.1073/pnas.0709145105
- 652 31. Rafiqi AM, Park C, Kwan CW, Lemke S, Schmidt-ott U. BMP-dependent serosa and
- amnion specification in the scuttle fly Megaselia abdita. 2012;3382: 3373–3382.
- 654 doi:10.1242/dev.083873
- 655 32. Kwan CW, Gavin-Smyth J, Ferguson EL, Schmidt-Ott U. Functional evolution of a
- 656 morphogenetic gradient. Bronner M, editor. Elife. eLife Sciences Publications, Ltd;
- 657 2016;5: e20894. doi:10.7554/eLife.20894

- 658 33. Caroti F, González Avalos E, González Avalos P, Kromm D, Noeske V, Wosch M, et al. In
- toto live imaging in scuttle fly Megaselia abdita reveals transitions towards a novel
- 660 extraembryonic architecture. bioRxiv. 2018; Available:
- 661 http://biorxiv.org/content/early/2018/01/15/236364.abstract
- 662 34. Jacobs CGC, Spaink HP, van der Zee M. The extraembryonic serosa is a frontier
- 663 epithelium providing the insect egg with a full-range innate immune response. Elife.
- 664 2014;3: 1–21. doi:10.7554/eLife.04111
- 665 35. Jacobs CGC, Van Der Zee M. Immune competence in insect eggs depends on the
- 666 extraembryonic serosa. Dev Comp Immunol. 2013;41. doi:10.1016/j.dci.2013.05.017
- 667 36. Lynch JA, Roth S. The evolution of dorsal-ventral patterning mechanisms in insects.
- 668 Genes Dev. 2011;25: 107–118. doi:10.1101/gad.2010711
- 669 37. Horn T, Panfilio KA. Novel functions for Dorsocross in epithelial morphogenesis in the
- 670 beetle Tribolium castaneum. Development. 2016;143: 3002–3011.
- 671 doi:10.1242/dev.133280
- 672 38. Anderson DT. The Development of Holometabolous Insects. In: Counce SJ, Waddinton
- 673 CH, editors. Developmental systems Insects, Vol 1. New York: Academic Press; 1972.
- 674 pp. 165–242.

- 675 39. Anderson DT. The Development of Hemimetabolous Insects. In: Counce SJ,
- 676 Waddington CH, editors. Developmental systems Insects, Vol 1. New York: Academic
- 677 Press; 1972. pp. 95–163.
- 40. Aranda M, Marques-Souza H, Bayer T, Tautz D. The role of the segmentation gene
- hairy in Tribolium. Dev Genes Evol. 2008;218: 465–77. doi:10.1007/s00427-008-0240-
- 680
- 681 41. Benton MA. Fluorescent live imaging of differentially labeled Tribolium embryos

682	[Internet]. Datab	ase: figshare [[Internet]. 2018.	Available:
-----	-------------------	-----------------	-------------------	------------

- 683 https://figshare.com/authors/Matthew_Benton/4693354
- 42. Tomancak P, Berman BP, Beaton A, Weiszmann R, Kwan E, Hartenstein V, et al. Global
- 685 analysis of patterns of gene expression during Drosophila embryogenesis. Genome
- 686 Biol. England; 2007;8: R145. doi:10.1186/gb-2007-8-7-r145
- 43. Hammonds AS, Bristow CA, Fisher WW, Weiszmann R, Wu S, Hartenstein V, et al.
- 688 Spatial expression of transcription factors in Drosophila embryonic organ
- 689 development. Genome Biol. England; 2013;14: R140. doi:10.1186/gb-2013-14-12-r140
- 690 44. Tomancak P, Beaton A, Weiszmann R, Kwan E, Shu S, Lewis SE, et al. Systematic
- 691 determination of patterns of gene expression during Drosophila embryogenesis.
- 692 Genome Biol. England; 2002;3: RESEARCH0088.
- 693 45. Sam S, Leise W, Hoshizaki DK. The serpent gene is necessary for progression through
- the early stages of fat-body development. Mech Dev. 1996;60: 197–205. Available:
- 695 http://www.ncbi.nlm.nih.gov/pubmed/9025072
- 696 46. Sachs L, Chen YT, Drechsler A, Lynch JA, Panfilio KA, Lässig M, et al. Dynamic BMP
- 697 signaling polarized by Toll patterns the dorsoventral axis in a hemimetabolous insect.
- 698 Elife. 2015;4. doi:10.7554/eLife.05502
- 699 47. Handel K, Basal A, Fan X, Roth S. Tribolium castaneum twist: gastrulation and
- mesoderm formation in a short-germ beetle. Dev Genes Evol. 2005;215: 13–31.
- 48. van der Zee M, Stockhammer O, von Levetzow C, Nunes da Fonseca R, Roth S.
- 702 Sog/Chordin is required for ventral-to-dorsal Dpp/BMP transport and head formation
- in a short germ insect. Proc Natl Acad Sci U S A. 2006;103: 16307–12.
- 704 doi:10.1073/pnas.0605154103
- 705 49. Stappert D, Frey N, von Levetzow C, Roth S. Genome-wide identification of Tribolium

706	dorsoventral	natterning	genes. Devel	onment 20)16·143·2	443-2454
700	0013000111101	patterning	genes. Deven	opinent. 20	,,,,,,,,,,,,,,,,,,,,,,,,,,,,,,,,,,,,,,,	TTJ 2TJT

- 707 doi:10.1242/dev.130641
- 708 50. van der Zee M, Benton MA, Vazquez-Faci T, Lamers GEM, Jacobs CGC, Rabouille C.
- 709 Innexin7a forms junctions that stabilize the basal membrane during cellularization of
- the blastoderm in Tribolium castaneum. Development. 2015;142: 2173–2183.
- 711 doi:10.1242/dev.097113
- 712 51. Rauzi M, Krzic U, Saunders TE, Krajnc M, Ziherl P, Hufnagel L, et al. Embryo-scale tissue
- 713 mechanics during Drosophila gastrulation movements. Nat Commun. The Author(s);
- 714 2015;6: 8677. Available: http://dx.doi.org/10.1038/ncomms9677
- 715 52. Leptin M, Grunewald B. Cell shape changes during gastrulation in Drosophila.
- 716 Development. 1990;110: 73 LP-84. Available:
- 717 http://dev.biologists.org/content/110/1/73.abstract
- 718 53. Roth S. Gastrulation in Other Insects. In: Stern CD, editor. Gastrulation From Cells to
- 719 Embryo. New York: Cold Spring Harbor Laboratory Press; 2004. pp. 105–121.
- 720 54. Ewen-Campen B, Jones TEM, Extavour CG. Evidence against a germ plasm in the
- 721 milkweed bug Oncopeltus fasciatus, a hemimetabolous insect. Biol Open. 2013;2:
- 722 556–68. doi:10.1242/bio.20134390
- 55. Erezyilmaz DF, Kelstrup HC, Riddiford LM. The nuclear receptor E75A has a novel pair-
- 724 rule-like function in patterning the milkweed bug, Oncopeltus fasciatus. Dev Biol.
- 725 Elsevier Inc.; 2009;334: 300–10. doi:10.1016/j.ydbio.2009.06.038
- 726 56. Liu PZ, Kaufman TC. even-skipped is not a pair-rule gene but has segmental and gap-
- 727 like functions in Oncopeltus fasciatus, an intermediate germband insect.

728 Development. 2005;132: 2081–92. doi:10.1242/dev.01807

729 57. Gillis WQ, Bowerman B a, Schneider SQ. The evolution of protostome GATA factors:

730		molecular phylogenetics, synteny, and intron/exon structure reveal orthologous
731		relationships. BMC Evol Biol. 2008;8: 112. doi:10.1186/1471-2148-8-112
732	58.	Nagai T, Ibata K, Park ES, Kubota M, Mikoshiba K, Miyawaki A. A variant of yellow
733		fluorescent protein with fast and efficient maturation for cell-biological applications.
734		Nat Biotechnol. Nature Publishing Group; 2002;20: 87. Available:
735		http://dx.doi.org/10.1038/nbt0102-87
736	59.	Clark E, Akam M. Odd-paired controls frequency doubling in Drosophila segmentation
737		by altering the pair-rule gene regulatory network. Elife. England; 2016;5.
738		doi:10.7554/eLife.18215
739	60.	Schindelin J, Arganda-Carreras I, Frise E, Kaynig V, Longair M, Pietzsch T, et al. Fiji: an
740		open-source platform for biological-image analysis. Nat Methods. 2012;9: 676–82.
741		doi:10.1038/nmeth.2019
742	61.	Meijering E, Dzyubachyk O, Smal I. Methods for cell and particle tracking. [Internet].
743		1st ed. Methods in enzymology. United States: Elsevier Inc.; 2012. doi:10.1016/B978-
744		0-12-391857-4.00009-4
745		
746		
747	S1 Fi	g. Results of photoconversions at 50% egg length. NLS-tdEos labelled extended
748	germ	band stage <i>Tribolium</i> embryos in which a patch of blastoderm nuclei were
749	photo	oconverted at 50% egg length (from the posterior pole) at different DV positions. The
750	approximate DV position of the patch and the approximate DV width of the clone (in terms	
751	of nu	clei number) are shown. The dorsal labelled embryo is shown from both sides to
752	demo	onstrate the photoconverted nuclei cover the full DV extent of the amnion (arrows).

753 Unconverted protein is shown in magenta, converted protein is shown in cyan. Images are

754 maximum intensity projections of one egg hemisphere. All eggs are oriented with the

- anterior to the left and ventral to the bottom. Scale bars are 100 μ m.
- 756

757	S2 Fig. Results of photoconversions at 25% egg length. NLS-tdEos labelled extended
758	germband stage Tribolium embryos in which a patch of blastoderm nuclei were
759	photoconverted at 25% egg length (from the posterior pole) at different DV positions. The
760	approximate DV position of the patch and the approximate DV width of the clone (in terms
761	of nuclei number) are shown. Unconverted protein is shown in magenta, converted protein
762	is shown in cyan. Images are maximum intensity projections of one egg hemisphere. All eggs
763	are oriented with the anterior to the left and ventral to the bottom. Scale bars are 100 μ m.
764	
765	S3 Fig. Results of photoconversions near the posterior pole. NLS-tdEos labelled extended
766	germband stage Tribolium embryos in which a patch of blastoderm nuclei were
767	photoconverted near the posterior pole at different DV positions. The approximate DV
768	position of the patch and the approximate DV width of the clone (in terms of nuclei number)
769	are shown. The second dorsally labelled embryo is shown at high magnification at two
770	timepoints and with a transverse section (at the position of the dashed green line) to show
771	the movement of tissue from the dorsal epithelium into the hindgut. Unconverted protein is
772	shown in magenta, converted protein is shown in cyan. Images are maximum intensity
773	projections of one egg hemisphere except for the bottom three embryos, which are shown
774	as maximum intensity projects through the germband in order to better show the labelled
775	nuclei. All eggs are oriented with the anterior to the left and ventral to the bottom except
776	for the second timepoint of the second dorsal view, which is shown with the posterior of the
777	germband to the left. Scale bars are 100 μ m.

779	S4 Fig. RNA expression of the Tribolium ortholog of the GATA factor serpent. (A-F) whole
780	mount and (G-J) flatmount <i>Tribolium</i> embryos from the pre-blastoderm to the retracting
781	germband stage stained for <i>Tc-srp</i> mRNA (red) and nuclei (DAPI, blue). (G ₁) and (G ₂) show
782	the same embryo imaged from both sides. (H $_1$) and (H $_2$) show projections from the dorsal
783	epithelium (H ₁) and the ventral epithelium (H ₂) of the same embryo. <i>Tc-srp</i> mRNA is
784	maternally provided (A), and expression is ubiquitous until the late blastoderm stage (B-C)
785	when expression clears from the blastoderm but persists in the yolk nuclei (scattered spots
786	in (D-E)). During embryo condensation, <i>de novo</i> expression arises in a patch of blastoderm
787	cells at the anterior medial region (arrowhead in F). This patch of <i>Tc-srp</i> expressing cells
788	invaginates as part of the ventral furrow and becomes located beneath the ectoderm
789	(arrowhead in G_1 - H_3). This expression domain is likely homologous to the anterior ventral
790	expression domain in <i>Drosophila</i> that marks the prohemocytes. During serosa window
791	closure, expression appears in a ring of dorsal epithelium cells (G $_1$). After serosa window
792	closure, expression persists in the dorsal epithelium (H $_1$) and (H $_3$). Unlike Drosophila, there is
793	no expression domain at the posterior of the blastoderm (E) or the early germband (G_2).
794	After germband elongation, a <i>de novo</i> expression domain appears at the posterior most
795	point of the embryo (I1). Given the location of this domain at the base of the forming
796	hindgut, this is likely the posterior endoderm primordium. Expression can also be seen in a
797	patch of amnion that has remained attached to the germband (arrow in I_2), but most of the
798	rest of the amnion has been lost. Several other regions of expression can be seen, including
799	in the presumptive fat body (the segmental domains running down the body), in
800	presumptive hemocyte clusters (the two side-by-side domains in the anterior), and in an
801	anterior domain that may mark the anterior endoderm primordium. Expression also persists

802 in the yolk nuclei (visible in the remaining yolk fragments at the anterior of the germband in 803 I_1). All embryos are shown with anterior to the left. (E-E'') is oriented with the ventral to the 804 bottom, (F-F'') is oriented as a ventral view. (H_3-H_3'') is an optical sagittal section at 805 approximately the midline of the embryo in (H_2) . (A-F) are maximum intensity projections of 806 one egg hemisphere. (G_1-G_2'') , (|1-|1'') and (J-J'') are maximum intensity projections of 807 flatmounted germbands. $(1_2-1_2'')$ is a maximum intensity projection of part of the germband 808 to better show the amnion/dorsal epithelium. Scale bars are 50 μ m. 809 S5 Fig. Schematics showing the photoconversion approach to determine the amnion 810 fatemap. A patch of nuclei (of known dimensions) was photoconverted at the blastoderm 811 stage, then the same embryos were examined at the end of germband extension. In 812 embryos where all photoconverted nuclei were located in the amnion and these nuclei 813 spanned the entire DV width of the amnion (as shown here), the number of nuclei initially 814 photoconverted was used to determine the DV width of the blastoderm domain giving rise 815 to the amnion. Note that the precise number and distribution of nuclei shown here were 816 arbitrarily chosen. Blue shows photoconverted nuclei, yellow shows the yolk. The serosa is 817 omitted from the bottom panels. 818 819 S6 Fig. Extended schematics showing the classic and revised *Tribolium* amnion fatemaps

fatemaps and germband models based on the results of this manuscript. The schematics of the flatmounted germbands are drawn with the focus on the dorsal epithelium. See text for additional details.

and germband models. Schematics drawn as in Fig 1 to show the classic and revised

824

820

825	S7 Fig. Tissue specific cell shape changes during Tribolium condensation. Stills from
826	timelapses of two Tribolium embryos transiently expressing GAP43YFP to label membranes.
827	The second panel of each timepoint shows optical transverse sections at the position of the
828	dashed line in the related panel. Ventral and lateral ectoderm becomes columnar, while
829	dorsal ectoderm becomes flattened. The non-columnar cells at the bottom of the left hand
830	embryo are likely the presumptive mesoderm. The first frame of the timelapses was defined
831	as timepoint 0. Both embryos are oriented with the anterior to the left and ventral to the
832	bottom. Abbreviations are: Dorsal (Dor), Lateral (Lat), Ventral (Ven) and Ectoderm (Ect).
833	Scale bars are 100 μm.
834	
835	
836	S1 Movie. Confocal timelapse of a <i>Tribolium</i> embryo transiently expressing H2B-ven to mark
837	nuclei. A maximum intensity projection of one egg hemisphere is shown. Anterior is to the
838	left, the ventral side of the egg is to the bottom.
839	
840	S2 Movie. Same timelapse as Supplementary Movie 1, but with nuclei of the dorsal
841	epithelium tracked until they join the ventral epithelium. Nuclei that join the ventral
842	epithelium are labelled magenta, nuclei that become located at the edge of the germband
843	are labelled yellow, nuclei that remain in the dorsal epithelium are labelled cyan. Anterior is
844	to the left, the ventral side of the egg is to the bottom. See Fig 2(A-C) for more details.
845	
846	S3 Movie. Same timelapse as Supplementary Movie 1, but with a line of nuclei of the dorsal
847	epithelium tracked. Nuclei that remain in the dorsal epithelium are labelled cyan. Anterior is

to the left, the ventral side of the egg is to the bottom. See Fig 2(D-F) for more details.

848

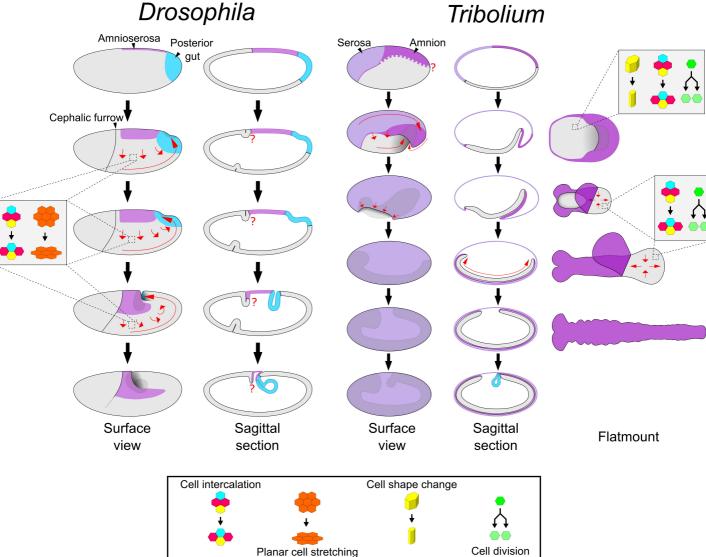
84	9
----	---

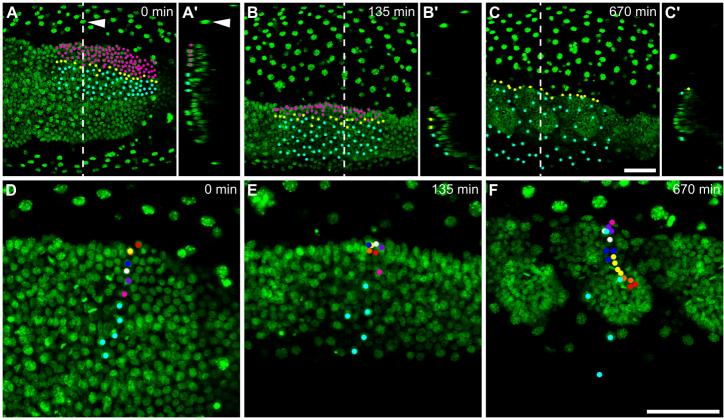
850	S4 Movie. Confocal timelapse of a <i>Tribolium</i> embryo transiently expressing NLS-tdEos
851	(magenta) with a line of blastoderm cells photoconverted (cyan). The brightness increases
852	approximately halfway through the movie due to a manual increase in laser power at this
853	point. A maximum intensity projection of one egg hemisphere is shown. Anterior is to the
854	left, the ventral side of the egg is to the bottom.
855	
856	S5 Movie. Confocal timelapse of a <i>Tribolium</i> embryo transiently expressing NLS-tdEos
857	(magenta) with a patch of blastoderm cells photoconverted (cyan). (A) shows a maximum
858	intensity projection of one egg hemisphere is shown. (B) shows an optical transverse section.
859	(C) shows an average intensity projection of 10 optical transverse sections. Anterior is to the
860	left, the ventral side of the egg is to the bottom. See Fig 3(A-F) for more details.
861	
862	S6 Movie. Confocal timelapse of a <i>Tribolium</i> embryo expressing NLS-tdEos showing the SAZ
863	during abdominal segment formation. Coloured points mark tracked nuclei. The embryo is
864	oriented based on polarity of the visible region of the germband with posterior to the right
865	and lateral to the top. Panels show maximum intensity projections of 15 μm to specifically
866	show the germband. See Fig 4 for more details.
867	
868	S7 Movie. Confocal timelapse of a <i>Tribolium</i> embryo transiently expressing NLS-tdEos
869	(magenta) with a patch of blastoderm cells photoconverted (cyan). Towards the end of the
870	timelapse, the cyan nuclei in the dorsal epithelium appear to condense posteriorly to the
871	hindgut. A maximum intensity projection of one egg hemisphere is shown. Anterior is to the

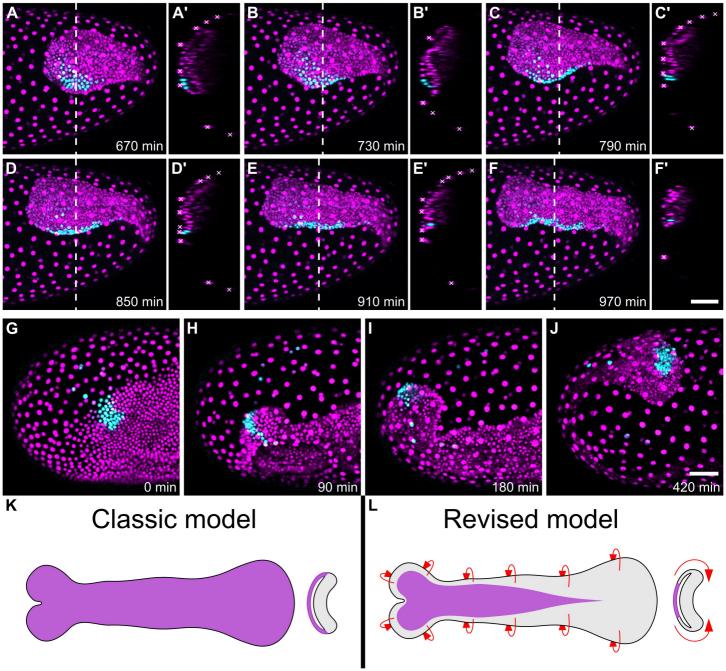
872 left, the ventral side of the egg is to the bottom.

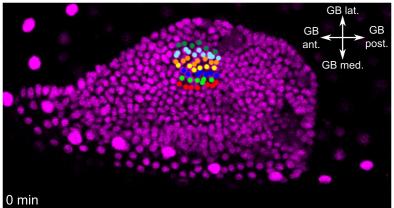
873

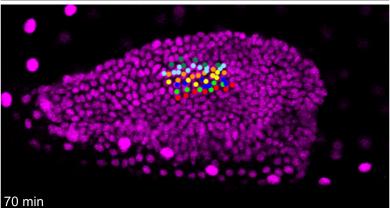
- 874 S1 Text. Extended discussion of topics from Discussion section 'A revised understanding of
- 875 the short germ embryo'.
- 876 S2 Text. Extended discussions of topics from Discussion section 'Cellular and molecular
- 877 causes of tissue flow'.
- 878 S3 Text. Extended discussions of topics from Discussion section 'Reconciling long and short
- 879 germ development'.

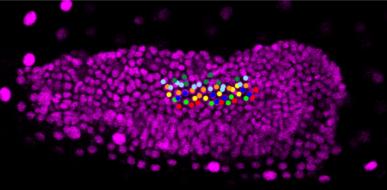




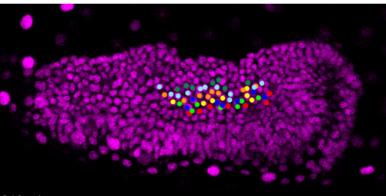












210 min

